Metallurgy and materials
*Metalurgia e materiais*

# Microstructural analysis in the Fe-30.5Mn-8.0Al-1.2C and Fe-30.5Mn-2.1Al-1.2C steels upon cold rolling

http://dx.doi.org/10.1590/0370-44672015690097

**Fabrício Mendes Souza**
Professor PhD - PEB
Secretaria de Estado de Educação de Minas Gerais
Belo Horizonte – Minas Gerais – Brasil
souzafm@yahoo.com.br

**Angelo Fernando Padilha**
Professor PhD
Universidade de São Paulo - USP
Escola Politécnica
Departamento de Engenharia Metalúrgica e de Materiais
São Paulo – São Paulo – Brazil
padilha@usp.br

**Ivan Gutierrez-Urrutia**
Senior Researcher
National Institute for Materials Science –
Research Center for Strategic Materials –
Microstructure Design Group
Japan - Tsukuba
gutierrezurrutia.ivan@nims.go.jp

**Dierk Raabe**
Director
Max-Planck-Institut fur Eisenforschung GmbH -
Department of Microstructure Physics
and Alloy Design
Dusseldorf – Germany
d.raabe@mpie.de

## Abstract

Electron backscatter diffraction (EBSD) and electron channeling contrast imaging (ECCI) were used to examine microstructural changes of the austenitic low-density Fe-30.5Mn-8.0Al-1.2C (8Al) and Fe-30.5Mn-2.1Al-1.2C (2Al) (wt.%) steels during cold rolling. As the strain increased, deformation mechanisms, such as stacking faults, slip, mechanical twinning, and shear banding were activated in both steels cold rolled up to strain of 0.69. Only slip was noted in these steels at low strain (ε=0.11) and slip dominance was detected in the 8Al steel at higher strains. Shear banding became active at higher strain (ε~0.7) in these materials. An inhomogeneous microstructure formed in both alloys at such strain level. More extensive mechanical twinning in the 2Al alloy than that in the 8Al alloy was observed. Fish bone-like structure patterns were revealed in the 8Al steel and a river-like structure in the 2Al steel. Detailed microstructure features as elongated and fragmented grains along the rolling direction (RD) were found for both steels, as already observed in other high-Mn steels. These deformed structures are composed by lamellar packets which can contain mechanical twins or slip lines and shear bands.

**Keywords:** Austenitic steels; Fe-Mn-C alloys; Fe-Mn-Al-C alloys; Microstructure; EBSD; ECCI; TWIP steels.

## 1. Introduction

Austenitic high manganese lightweight steels have an excellent combination of strength and ductility (ultimate tensile strength: 1.0-1.5 GPa and elongation: 30-80%) at room temperature, due to the occurrence of different hardening mechanisms in their deformed microstructures, which were here characterized during cold rolling. These steels are good candidates for structural application purposes in the automobile industry (GUTIERREZ-URRUTIA and RAABE, 2012, 2013). Al addition in Fe-Mn-C alloys increases the corrosion resistance of austenitic steels, and causes precipitation of nano-sized $(Fe,Mn)_3AlC$ carbides (with an average size of 10 x 20 nm), which control the mechanical properties of the alloys in the Fe-Mn-Al-C system. Carbon is an austenite stabilizer and strengthener of these alloys. Dislocation substructure refinement and subsequent activation of deformation twinning (Twinning Induced Plasticity, TWIP effect) play a significant role in the strain-hardening of the Fe-30.5Mn-2.1Al-1.2C (wt.%) alloy. In the TWIP phenomenon, nucleated deformation twins gradually continue to emerge, increasing the amount of smaller new twins and acting as obstacles to gliding dislocations in the deformed microstructure (CHRISTIAN and MAHAJAN, 1995; BOUAZIZ *et al*, 2011), with increasing strain (Hall-Petch effect). Strain hardening in the Fe-30.5Mn-8.0Al-1.2C alloy is also attributed to precipitation of κ–carbides and their role on the planar dislocation substructure development (HUANG *et al*, 1994; GUTIERREZ-URRUTIA and RAABE, 2012; PARK, 2012). To avoid intergranular precipitation, alloying addition should be limited to within about 5.5 wt.% Al and 0.67

wt.% carbon, so as to avoid intragranular precipitation in alloys of the Fe-Mn-Al-C system, Al addition needs to be limited to about 6.2 wt.%, and carbon to about 1.0 wt.% (HUANG *et al*, 1994). Wide stacking faults bounded by partial dislocations with smaller partial separation and delay mechanical twinning have been observed in the Fe-22Mn-3Al-0.6C steel, mainly due to its higher stacking fault energy, SFE, compared to that of the 0Al steel (PARK *et al*, 2010). The Fe-30.5Mn-8.0Al-1.2C steel has an SFE of 63 mJ $m^{-2}$ (GUTIERREZ-URRUTIA and RAABE, 2012). We may estimate a high SFE of 80-110 mJ $m^{-2}$ for the Fe-30.5Mn-8.0Al-1.2C alloy studied here, as observed in the alloy sort with composition range of Fe-(28±2)Mn-(10±2)Al-(1±0.2)C (wt.%) (PARK, 2012). The dependence of mechanical properties and deformation mechanisms has been examined in TWIP steels of the Fe-Mn-C system by different research groups (VERCAMMEN *et al*, 2004; BARBIER *et al*, 2009; BOUAZIZ *et al*, 2011; LÜ *et al*, 2011; DE COOMAN *et al*, 2011). High-Mn TWIP steels have been considerably explored, while the Fe-30.5Mn-8.0Al-1.2C (8Al) and Fe-30.5Mn-2.1Al-1.2C (2Al) alloys have been studied only in the tensile-tested condition up to now (GUTIERREZ-URRUTIA and RAABE, 2012, 2013). Hence, the microstructure evolution in these austenitic 8Al and 2Al steels remain up to now not studied under the cold rolling condition. The aim of this work is to analyze the microstructure changes and associate them with the activated deformation mechanisms with progressing strain, owing to their high and medium SFE, respectively, as well as, assimilate them with some already studied cold-rolled Fe-Mn-C alloys. We performed the microstructure characterization of the 8Al and 2Al steels by using electron backscatter diffraction (EBSD) and electron channeling contrast imaging (ECCI).

## 2. Materials and methods

The chemical compositions of the steels were Fe-30.5Mn-8.0Al-1.2C and Fe-30.5Mn-2.1Al-1.2C (wt. %). Details on alloy processing can be found in (GUTIERREZ-URRUTIA and RAABE, 2013). The 8Al alloy may present intragranular nano-sized κ–carbide precipitates (HUANG *et al*, 1994; PARK, 2012; GUTIERREZ-URRUTIA and RAABE, 2013). The alloys were subsequently cold rolled down to thickness reductions with ε=0.11; 0.22; 0.36; 0.51; 0.69 (Figure 1). The steels were cold rolled up to 50% thickness reduction because the maximum force of the used laboratory rolling mill was not sufficient to further reduce the thickness of the specimens. Microstructures of the cold rolled materials were determined by the electron backscatter diffraction (EBSD) technique with step size of 5 μm from different regions on the specimens (with surface area of about 70 $mm^2$), reaching scanned total area of about 8 $mm^2$ in size for each sample. High resolution Kikuchi pattern images were scanned with step size of about 0.1 μm to microtexture analysis. The EBSD measurements were performed by a 6500 F JEOL field emission gun scanning electron microscope (FEG-SEM) equipped with a TSL OIM EBSD software system. EBSD scans were carried out on the specimen's plane surface, parallel to the rolling direction (RD) and normal direction (ND). The microscope was operated at 15 kV acceleration voltage and 15 mm working distance. Kikuchi pattern image quality (IQ) maps and Kernel average misorientation (KAM) maps were obtained by means of TSL-OIM software calculation to compose the microstructures. The mapping was realized through the misorientation measurement between a grain at the Kernel center and all points (third nearest neighbors) at the Kernel's perimeter in KAM map. The local misorientation value assigned to the center point is the average of these misorientations. The KAM map illustrates how the local deformation energy was accommodated on the deformed microstructure. The deformation mechanisms in the microstructure of the 8Al steel specimens were characterized by using the electron channeling contrast imaging (ECCI) technique combined with EBSD. This approach has been successfully applied to the characterization of dislocation and twin substructures in high-Mn steels. ECCI observations were carried out in a Zeiss Crossbeam instrument (XB 1540, Carl Zeiss SMT AG, Germany). Details on EBSD-based set-up used to obtain ECCI images can be found in (GUTIERREZ-URRUTIA *et al*, 2009).

## 3. Results

Cold rolling microstructures are shown on the Kikuchi pattern image quality (IQ) and Kernel average misorientation (KAM) maps in Figure 1, which revealed that the hot-rolled materials is fully austenitic, i.e. fcc phase, containing equiaxed grains with grain size of 148 μm (8Al) and 102 μm (2Al). Figure 1 shows IQ maps of the 8Al and 2Al high-Mn steels cold rolled up to strain of 0.69, exhibiting the evolution of the deformed structures. It can be observed that the grains start to elongate and to fragment, resulting in a structure of grains elongated along the rolling direction (RD) with a fish bone-like structure patterns revealed in the 8Al steel, and a river-like structure in the 2Al steel, at the higher strain level, as already found in some high-Mn steels (VERCAMMEN *et al*, 2004; LÜ *et al*, 2011). These structures are composed by lamellar packets (Figure. 1), which can contain stacking faults, slip lines, mechanical twins, and even shear bands. High resolution IQ maps in Figure 2(a)-(c) illustrate the main microstructure features of the 8Al steel at cold rolling degrees of 10%, 20%, and 50% reductions, and those of the 2Al steel at 10%, 40%, and 50% reductions are shown in Figure 2(d)-(f), respectively. In Figure 2 the red lines on the IQ maps denote the Σ3 twin boundaries, and the black lines indicate the high angle grain boundaries.

The images concerning the KAM maps show the evolution of local deformation energy in the deformed microstructures of the 8Al steel at 10% and 50% reductions in Figure 3(a) and (b), as well as those of the 2Al steel also at 10% and 50% reductions in Figure 3(c) and (d), respectively. Similar aspects were observed in a MnCu alloy, where the dislocation structure changes from a homogeneous arrangement to a strongly heterogeneous one

during deformation, and areas with small and large KAM represent low and high dislocation densities respectively (ZHONG *et al*, 2007). The evolution process of the substructures from the homogeneous arrangement to the heterogeneous one is clearly observed in both steels (Figure 3).

Deformation twins were not detected on the IQ maps, where slip lines can be observed, and only remaining annealing twins were seen in both 8Al and 2Al steels at 10% reduction, as shown in Figures 2(a) and (d). This indicated that slip is responsible for accommodation of plastic deformation energy at lower strain in such steels. It has been reported that two layer stacking faults act as a twin nucleus, and secondary polar sources created by the interaction of perfect dislocations with the Shockley twinning partials, probably control the twin growth. Furthermore, the mechanical twins, containing a high level of sessile dislocations, improve the composite strengthening effect in the Fe-Mn-C, Hadfield-related, TWIP steels (IDRISSI *et al*, 2010). Accordingly, deformation twins are formed on slip traces to accommodate further plastic deformation at higher strain levels in both 8Al and 2Al steels (Figure 2). Deformation twinning was activated in the tensile-deformed 2Al steel at 0.2 true strain/950 MPa (GUTIERREZ-URRUTIA and RAABE 2012).

Other authors (DONADILLE *et al*, 1989) realized that in 316 L austenitic stainless steel, deformation twins formed on {111} planes, which was attributed to preferential slip of both the matrix and twin components on the common aligned {111} twinning planes, as observed in these steels (Figure 2 and Figure 5). The {hkl} planes were here defined by selecting {111} in the inter-active view in the TSL software. The 1 and 2 arrows on the maps in Figure 2(b) and (c) were marked to reproduce their respective misorientation profile graphs shown in Figure 4(a) and (b), respectively. Curves on the graphs in Figure 4 show occurrence of mechanical twins, which can be differentiated from slip lines, since the rotation of the parent crystal around a <111> axis through an angle of 60° crystallographically describes the Σ3 twin in f.c.c. alloys. Deformation twinning in matrix was detected in the 8Al sample at 20% reduction (Figures 2(b) and 4(a)), which may be related to the theory of emissary slip (CHRISTIAN and MAHAJAN, 1995) that implies a physical separation of the shape change associated with twin formation and the change of lattice orientation, where one of the twin interfaces intersected the free surface in a series of zig-zag markings, Figures 2(b).

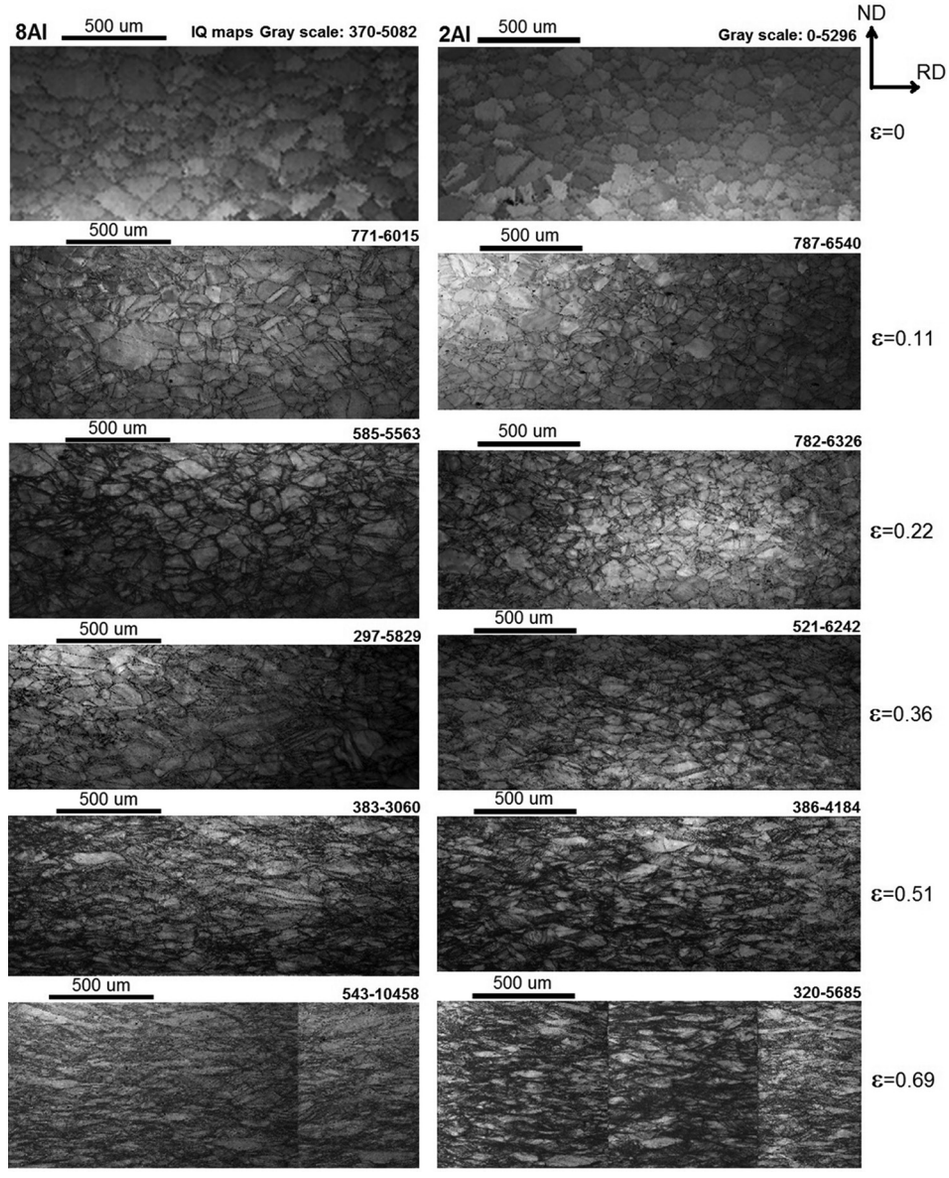


Figure 1
Image quality maps showing the deformation microstructures of the hot-rolled (ε=0) and cold-rolled 8Al and 2Al steels with progressing ε. RD: rolling direction and ND: normal direction.

The onset of non-crystallographic shear band (SB) formation can be also noted at higher strain (Figures 2(c) and (f)) in both 8Al and 2Al alloys as observed in other steels (DONADILLE *et al*, 1989; VERCAMMEN *et al*, 2004; LÜ *et al*, 2011). KAM maps in Figure 3 indicated that the non-dissipated energy in the deformed microstructures was stored mainly in low-angle grain boundaries, and evidenced a relative homogeneity of the deformed microstructures at low deformation level, as indicated by the small variation in the labeled gray scale on the KAM plots, whereas, at high deformation level, part of the plastic deformation energy was stored on deformation twins and on shear bands, indicating the occurrence of the microstructural heterogeneities in the 8Al steel, Figure 2(c), and more markedly those in the 2Al steel, Figure 2(f). This is also indicated by the increased KAM angle range on the KAM maps (Figure 3(b) and (d)) of the samples deformed to strain of about 0.7. As observed in Figure 2, dislocation slip was predominant in the 8Al steel, even at higher strains (~0.7), while slip and profuse mechanical twinning was observed in the 2 Al steel at such strain level.

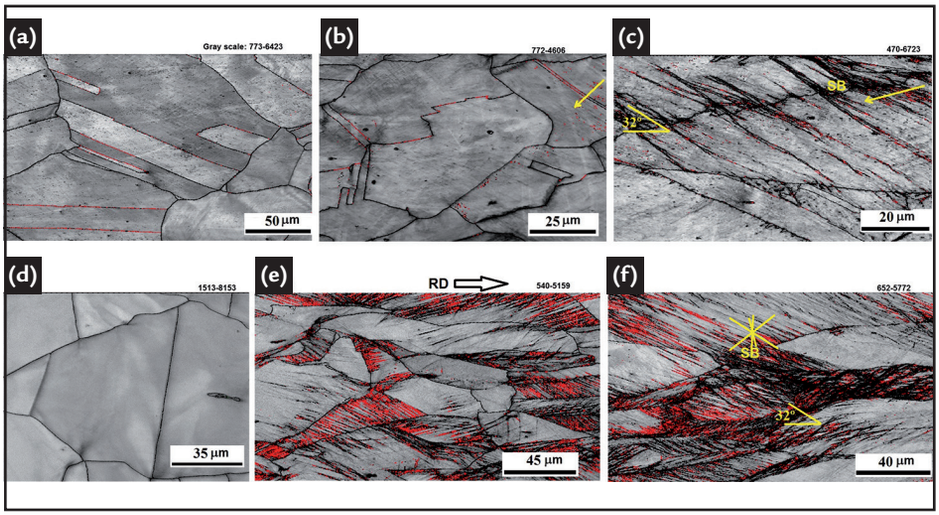


Figure 2
IQ maps of the samples cold-rolled down to (a) 10%, (b) 20%, and (c) 50% thickness reductions of the 8Al steel, and down to (d) 10%, (e) 40%, and (f) 50% thickness reductions of the 2Al steel. The red lines indicate the Σ3 twin boundaries, and the black lines denote the high angle grain boundaries. X-like marks in (f) represent {111} plane traces (They were drawn on the specified plane for the datapoint selected on the EBSD map. The length of the traces drawn is proportional to the inclination of the plane relative to the sample surface. The more inclined the plane the longer the trace). RD – Rolling direction.

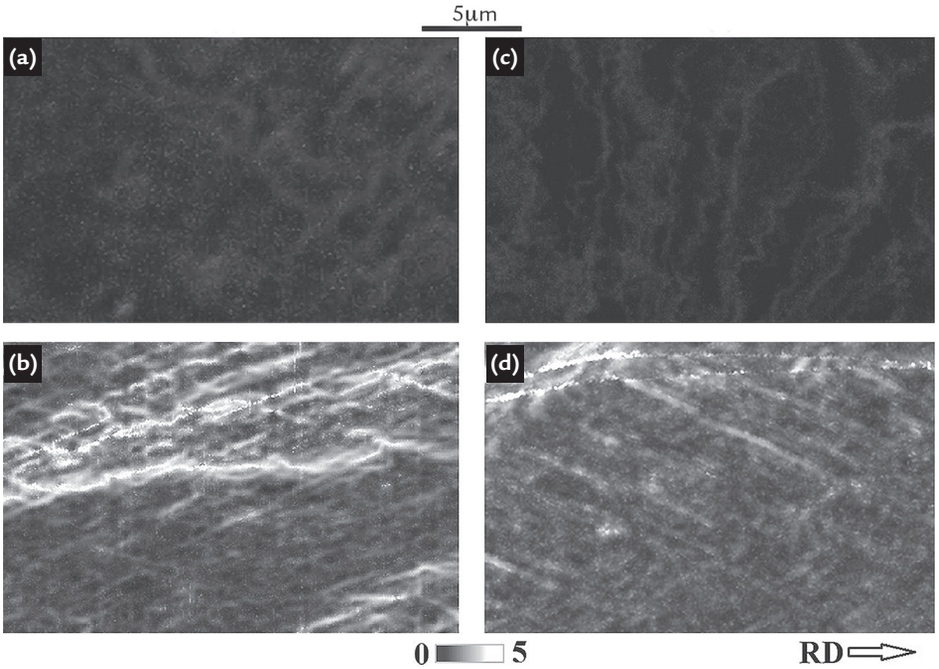


Figure 3
KAM maps of the cold-rolled samples at (a) 10% and (b) 50% thickness reductions for the 8Al steel, and at (c) 10% and (d) 50% thickness reductions for the 2Al steel. The KAM angle range is from 0° to 5°. RD represents the rolling direction.

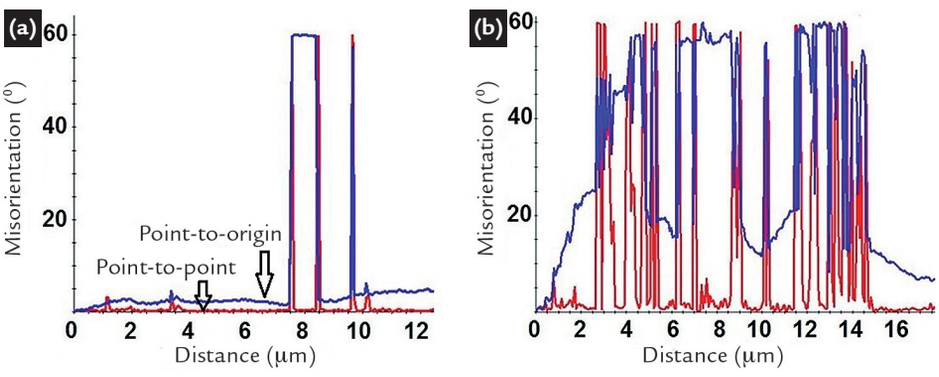


Figure 4
Misorientation profile graphs plotted along the arrows marked on the IQ maps in (a) Figure 2b and (b) Figure 2c for the 8Al steel.

## 4. Discussion

The microstructural changes is attractive for the insight of the resultant extreme mechanical properties of the rolled high-Mn austenitic steels, owing mainly to the dislocation refinement and deformation twinning development (TWIP effect), where the enhancement of strength and ductility is associated with the deformation mechanisms of γ-phase, depending on SFE. As detected in Figure 2(a) and (d), deformation twins were not observed at low strain (~0.1), where only slip was observed for both steels. In order to clarify the presence of deformation mechanisms at low and medium strains in the 8Al steel at strain levels of 0.22 (Figure 5(a)) and 0.69 (Figure 5(b)), ECCI images were obtained to show the occurrence of stacking faults, planar dislocation structures, mechanical twins, and shear bands. The high carbon and Al contents in the Fe-30.5Mn-8.0Al-1.2C (wt%) steel corroborate to precipitation (even in water quenched samples) of κ-carbides (PARK, 2012), which stabilizes planar dislocation substructures (HUANG *et al*, 1994; PARK *et al*, 2010; PARK, 2012; GUTIERREZ-URRUTIA and RAABE, 2013). ECCI images in Figure 5a shows that, in the 8Al steel sample at ε=0.22, grains identified as Grain 1, Grain 2, Grain 3, and Grain 4 have stacking faults and dislocation planar substructures, with slip on the operative {111} planes, indicating the dominance of slip. This suggests the possibility of planar slip stabilized by intragranular precipitation of nano-sized carbides in such steel. Further deformation twinning and shear banding were also observed at higher strain (Figure 5b). The ECCI image in the inferior right corner in Figure 5(b) is the increased magnification image from the marked area in the ECCI micrograph of Grain 3. Mechanical twins and shear bands (SB) were found in different grains (Grain 1, Grain 2, and Grain 3), where a bundle of twins inside shear bands, Figure 5(b), were also observed. These microstructural features are known as Cu-type shear bands that form the herring bone structure (Figure 1), and the well-established retainment of Goss orientation texture in the shear bands in the microstructure, as also found in other f.c.c. alloys (DONADILLE *et al*, 1989). An overshooting/latent-hardening effect can be caused by the closely spaced twin lamellae. When this effect is caused by the twin lamellae, the onset of shear banding can occur (LEFFERS and RAY, 2009), as observed in the 2Al steel (Figure 2(e) and (f)) and in the 8Al steel (Figure 5(a)-(d)). As a result, the inhomogeneous microstructures emerge at higher strain level for both steels, and more markedly in the 2Al steel, as can be seen in Figure 2(c) and (f), where twinning activity of Σ3 twins, represented by the red lines, is more intensive in the 2Al steel than that found in the 8Al steel, owing to its high amount of Al added as alloying element, reducing twin formation. This occurs because the critical resolved shear stress required for twin formation increases with increasing SFE (PARK *et al*, 2010). When twinning became an additional important mode of deformation in Ni-40%Co alloy, extensive deformation twinning was activated in different deformation stages as primary and secondary twins in the α-brass and MP35N alloys (ASGARI *et al*, 1997). The 2Al alloy may have these different deformation stages, as also investigated in such tensile-deformed alloy in previous work (GUTIERREZ-URRUTIA and RAABE, 2012). On the other hand, the 8Al alloy has delay mechanical twinning, diminishing the number of deformation stages on such steel compared to those on the 2Al steel at the same strain range. Non-crystallographic shear bands (usually oriented at 25-35° to the RD) and in matrix, has been observed in some f.c.c. alloys. Furthermore, shear banding and occurrence of structures of twins were observed in a 316 L austenitic stainless steel at 70% thickness reduction (DONADILLE *et al*, 1989). Accordingly, these microstructure features appeared in the 2Al steel and in the 8Al steel (Figure 2(c) and (f))) at ε=0.69, where shear bands and mechanical twins were observed. It was reported that the twin lamellae lattice distortion and shear banding are plastic instabilities, where deformation tends to concentrate in twinned areas, resulting in strongly inhomogeneous microstructures in Fe-Mn-Al-C alloys, with an increased stored energy (DONADILLE *et al*, 1989; LÜ *et al*, 2011), such as those identified in the microstructures of both steels by means of KAM maps, as shown in Figure 2(c) and (f) and Figure 3(b) and (d). This geometrically strengthened structure is caused by the Schmid factor for slip, decreased towards zero (twin plane), on the operative planes (VERCAMMEN *et al*, 2004). These deformation mechanisms can homogeneously be formed/adjusted in TWIP steels during the tensile and cup forming tests (used in automobile industries), optimizing technological properties in cup formability. In summary, planar dislocation structures and few mechanical twins developed at 10%-40% reduction in the 8Al and further SB at 50 %, while for the 2Al steel slip lines and profuse mechanical twins developed at 10%-40% reduction and further SB at 50%.

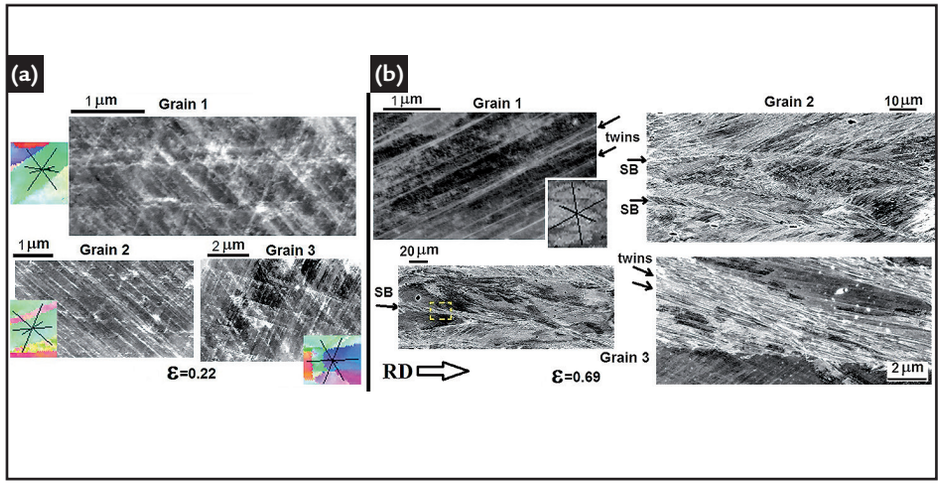


Figure 5
ECCI images of the 8Al steel samples at (a) ε=0.22 and at (b) ε=0.69 for different grains (right inferior corner ECCI image is from enlarged SB region of the Grain 3). X-like marks represent {111} plane traces (They were marked on the specified plane for the datapoint selected on the EBSD maps on the grains where their ECCI images were obtained. The length of the traces drawn is proportional to the inclination of the plane relative to the sample surface. The more inclined the plane the longer the trace). RD – Rolling direction.

## 5. Conclusions

Microstructural modification was examined in the two cold rolled low-density high-Mn steels, namely, Fe-30.5Mn-2.1Al-1.2C and Fe-30.5Mn-8.0Al-1.2C (wt%). EBSD observations indicated that stacking faults, slip lines, mechanical twins, and shear bands were found as the main microstructural features in both steels. Planar dislocation substructures were observed at low strain level in the 8Al steel, in addition to mechanical twins and shear banding, with a bundle of twins, formed in its microstructure at higher strain (50% reduction). Increase of mechanical twinning and shear banding were associated to a relatively microstructural heterogeneity development in the steels at higher strains. It was suggested that Al addition can be attributed to the planar dislocation formation, which was favored by sheared κ-carbides in the Fe-Mn-Al-C alloy with a higher amount of Al (8wt%). Twinning activity was more intensive in the 2Al steel, owing to its lower SFE. This behavior is similar to that found in TWIP steels belonging to the Fe-Mn-C system.

## 6. Acknowledgments

The authors acknowledge the financial support by the Science without Borders, Brazil's scholarship program, for the CNPq postdoctoral fellowship (process number: 237863/2012-0), and by the German Research Foundation in the framework of the SFB 761 – steel ab initio.

## 7. References

ASGARI, S., EL-DANAF, E., KALIDINDI, S. R., DOHERTY, R. D. Strain hardening regimes and microstructural evolution during large strain compression of low stacking fault energy fcc alloys that form deformation twins. ***Metallurgical and Materials Transactions A.*** v. 28A, 1781-1795, 1997.

BOUAZIZ, O., ALLAIN, S., SCOTT, C.P., CUGY, P., BARBIER, D. High manganese austenitic twinning induced plasticity steels: A review of the microstructure properties relationships. ***Current Opinion in Solid State and Materials Science.*** v. 15, p. 141-168, 2011.

BARBIER, D., GEY, N., BOZZOLO, N., ALLAIN, S., HUMBERT, M. EBSD for analyzing the twinning microstructure in fine-grained TWIP steels and its influence on work hardening. ***Jounal of Microscopy.*** 2009, vol. 235, pp. 67-78.

CHRISTIAN, J. W., MAHAJAN, S. Deformation Twinning. ***Progress in Materials Science.*** v. 39, p. 1–157, 1995.

DONADILLE, C., VALLE, R., DERVIN, P., PENELLE, R. Development of texture and microstructure during cold-rolling and annealing of f.c.c. alloys: example of an austenitic stainless steel. ***Acta Metallurgica et Materialia.*** v. 37, p. 1547-1571, 1989.

DE COOMAN, B. C., CHIN, K.-G., KIM, J. High Mn TWIP Steels for Automotive Applications. ***New Trends and Developments in Automotive System Engineering.*** p. 101-128, 2011.

GUTIERREZ-URRUTIA, I., RAABE, D. Multistage strain hardening through dislocation substructure and twinning in a high strength and ductile weight-reduced Fe–Mn–Al–C steel. ***Acta Materialia.*** v. 60, p. 5791–5802, 2012.

GUTIERREZ-URRUTIA, I., RAABE, D. Influence of Al content and precipitation state on the mechanical behavior of austenitic high-Mn low-density steels. ***Scripta Materialia.*** v. 68, p. 343-347, 2013.

GUTIERREZ-URRUTIA, I., ZAEFFERER, S., RAABE, D. Electron channeling contrast imaging of twins and dislocations in twinning-induced plasticity steels under controlled diffraction conditions in a scanning electron microscope. ***Scripta Materialia.*** v. 61, p. 737–740, 2009.

HONG, S., SHIN, S. Y., KIM, H. S., LEE, S., KIM, S.-K., CHIN, K.-G., KIM, N. J. Effects of aluminum addition on tensile and cup forming properties of three twinning induced plasticity steels. ***Metallurgical and Materials Transactions A.*** v. 43, pp. 1870-1883, 2012.

HUANG, H., GAN, D., KAO, P. W. Effect of alloying additions on the κ phase precipitation in an austenitic Fe-Mn-Al-C alloys. ***Scripta Metallurgica et Materialia.*** v. 30, p. 449-504, 1994.

IDRISSI, H., RENARD, K., RYELANDT, L., SCHRYVERS, D., JACQUES, P. J. On the mechanism of twin formation in Fe-Mn-C TWIP steels. ***Acta Materialia.*** v. 58, p. 2464-2476, 2010.

LEFFERS, T., RAY, R. K. The brass-type texture and its deviation from the copper-type texture. ***Progress in Materials Science.*** v. 54, p. 351-396, 2009.

LÜ, Y., MODOLOV, D. A., GOTTSTEIN, G. Correlation between microstructure and texture development in a cold-rolled TWIP steel. ***ISIJ International.*** v. 51, p. 812–817, 2011.

PARK, K.-T. Tensile deformation of low-density Fe–Mn–Al–C austenitic steels at ambient temperature. ***Scripta Materialia.*** 2012, http://dx.doi.org/10.1016/j.scriptamat.2012.09.031.

PARK, K.-T., JIN, K. G., HAN, S. H., HWANG, S. W., CHOI, K., LEE C. S. Stacking fault energy and plastic deformation of fully austenitic high manganese steels: Effect of Al addition. ***Materials Science and Engineering A.*** v. 527, p. 3651-3661, 2010.

VERCAMMEN, S., BLANPAIN, B., DE COOMAN, B.C., WOLLANTS, P. Cold rolling behaviour of an austenitic Fe–30Mn–3Al–3Si TWIP-steel: the importance of deformation twinning. ***Acta Materialia.*** v. 52, p. 2005–2012, 2004.

ZHONG, Y., YIN, F., SAKAGUCHI, T., NAGAI, K., YANG K. Dislocation structure evolution and characterization in the compression deformed Mn-Cu alloy. ***Acta Materialia.*** v. 55, p. 2747-2756, 2007.

Received: 06 July 2014 - Accepted: 10 March 2016.